Dynamically Reshaping Signaling Networks to Program Cell Fate via Genetic Controllers

Kate E. Galloway *et al.*

Science **341**, (2013);
DOI: 10.1126/science.1235005

Science (print ISSN 0036-8075; online ISSN 1095-9203) is published weekly, except the last week in December, by the American Association for the Advancement of Science, 1200 New York Avenue NW, Washington, DC 20005.

Dynamically Reshaping Signaling Networks to Program Cell Fate via Genetic Controllers

Kate E. Galloway, Elisa Franco, Christina D. Smolke*

READ THE FULL ARTICLE ONLINE
http://dx.doi.org/10.1126/science.1235005

Cite this article as K. E. Galloway *et al.*, *Science* **341**, 1235005 (2013).
DOI: 10.1126/science.1235005

Introduction: Engineering of cell fate through synthetic gene circuits requires methods to precisely implement control around native decision-making pathways and offers the potential to direct developmental programs and redirect aberrantly activated cell processes. We set out to develop molecular network diverters, a class of genetic control systems, to activate or attenuate signaling through a mitogen-activated protein kinase (MAPK) pathway, the yeast mating pathway, to conditionally route cells to one of three distinct fates.

Methods: We used a combination of genetic elements—including pathway regulators, RNA-based transducers, and constitutive and pathway-responsive promoters—to build modular network diverters. We measured the impact of these genetic control systems on pathway activity by monitoring fluorescence from a transcriptional pathway reporter. Cell fate determination was measured through halo assays, in which mating-associated cell cycle arrest above a certain concentration of pheromone from wild-type cells results in a "halo" or cleared region around a disk saturated in pheromone. A phenomenological model of our system was built to elucidate design principles for dual diverters that integrate opposing functions while supporting independent routing to alternative fates.

Results: We identified titratable positive (Ste4) and negative (Msg5) regulators of pathway activity that result in divergent cell fate decisions when controlled from network diverters. A positive diverter, controlling Ste4 through a feedback architecture, routed cells to the mating fate, characterized by pathway activation in the absence of pheromone. A negative diverter, controlling Msg5 through a nonfeedback architecture, routed cells to the nonmating fate, characterized by pathway inhibition in the presence of pheromone. When integrated into a dual-diverter architecture, the opposing functions of these positive and negative diverters resulted in antagonism, which prevented independent routing to the alternative fates. However, a modified architecture that incorporated both constitutive and feedback regulation over the pathway regulators enabled conditional routing of cells to one of three fates (wild type, mating, or nonmating) in response to specified environmental signals.

Discussion: Our work identified design principles for networks that induce differentiation of cells in response to environmental signals and that enhance the robust performance of integrated mutually antagonistic genetic programs. For example, integrated negative regulators can buffer a system against noise amplification mediated through positive-feedback loops by providing a resistance to amplification. Negative feedback can play an important role by reducing population heterogeneity and mediating robust, long-term cell fate decisions. The dual-diverter configuration enables routing to alternative fates and minimizes impact on the opposing diverter by integrating differential regulatory strategies on functionally redundant genes. Molecular network diverters provide a foundation for robustly programming spatial and temporal control over cell fate.

FIGURES IN THE FULL ARTICLE

Fig. 1. Molecular network diverters and key pathway control points.

Fig. 2. A synthetic biology toolbox for constructing molecular network diverters.

Fig. 3. Optimized design of independent positive and negative diverters.

Fig. 4. Integration of opposing diverters optimized for independent cell-fate routing results in antagonism.

Fig. 5. Optimizing the dual-diverter architecture and components for the integration of opposing diverters.

Fig. 6. Conditional routing of genetically identical cells containing a dual diverter to diverse fates in response to distinct environmental signals.

SUPPLEMENTARY MATERIALS

Materials and Methods
Supplementary Text
Figs. S1 to S14
Tables S1 to S17
References

RELATED ITEMS IN *SCIENCE*

C. A. Sarkar, Concentrating (on) natural signaling proteins for synthetic control of cell fate. *Science* **341**, 1349–1350 (2013).
DOI: 10.1126/science.1243994

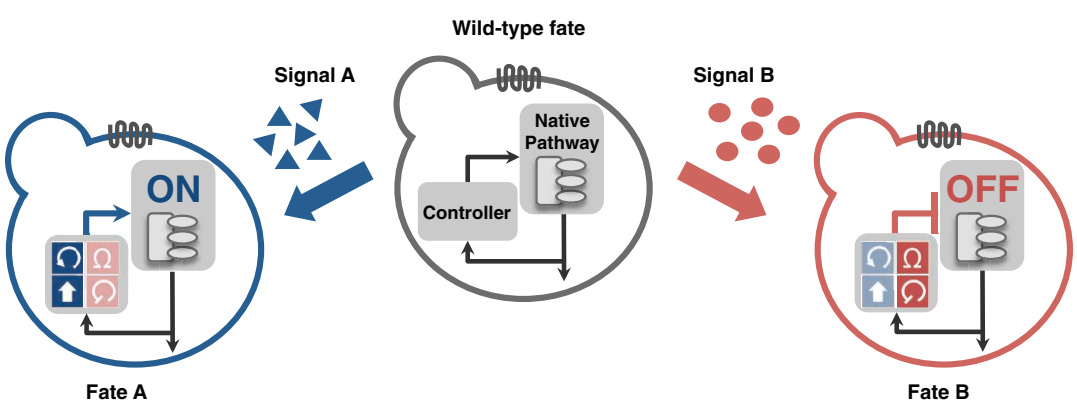

The molecular network diverter (controller) interfaces with a native signaling pathway to conditionally route cells to one of three fates in response to distinct environmental signals. Signal A (**left**) and signal B (**right**) trigger the positive and negative elements of the diverter via their cognate transducers to activate or inhibit, respectively, signaling through the yeast mating pathway.

The list of author affiliations is available in the full article online.
*Corresponding author. E-mail: christina.smolke@stanford.edu

Dynamically Reshaping Signaling Networks to Program Cell Fate via Genetic Controllers

Kate E. Galloway,[1] Elisa Franco,[2] Christina D. Smolke[3]*

Engineering of cell fate through synthetic gene circuits requires methods to precisely implement control around native decision-making pathways and offers the potential to direct cell processes. We demonstrate a class of genetic control systems, molecular network diverters, that interface with a native signaling pathway to route cells to divergent fates in response to environmental signals without modification of native genetic material. A method for identifying control points within natural networks is described that enables the construction of synthetic control systems that activate or attenuate native pathways to direct cell fate. We integrate opposing genetic programs by developing network architectures for reduced antagonism and demonstrate rational tuning of performance. Extension of these control strategies to mammalian systems should facilitate the engineering of complex cellular signaling systems.

Organisms orchestrate complex, coordinated tasks by dynamically programming the extracellular space with distributed molecular signals that are processed by individual cells into concerted responses (*1*–*3*). Programmed cells can harness sophisticated and complex biological processes to direct developmental programs and redirect aberrantly activated cell processes (*4*–*10*). The engineering of biological systems to regulate cell fate requires precise control over gene circuit performance (*11*, *12*) and the ability to interface with key decision-making pathways (*13*). Advances in synthetic biology may facilitate the design of sophisticated genetic circuits capable of sensing and actuating changes in native signaling networks (*14*).

Mitogen-activated protein kinase (MAPK) pathways are a class of signaling pathways that control such key cellular processes as differentiation, mitosis, and apoptosis (*1*). Many diseases, including one-third of human cancers, result from aberrant signaling through MAPK pathways (*15*, *16*). Conservation of the form and function of MAPK pathways has facilitated the translation of principles identified in yeast to higher eukaryotes (*17*, *18*). In the model organism *Saccharomyces cerevisiae*, pheromone stimulates cells to activate a three-tiered MAPK cascade that increases transcription of mating genes, induces cell cycle arrest, and initiates polarized cell growth. Synthetic circuits can be constructed with pathway-responsive promoters to form feedback control systems that directly prescribe dynamic pathway activation profiles (*19*, *20*). Chimeric protein scaffolds can also be used to route cells to alternative pathway responses (*21*). Although successful in modulating pathway activity or fate or both, these strategies primarily rely on genetic knockouts of endogenous genes, which can alter wild-type behavior and are difficult to implement in higher eukaryotes such as humans.

Interfacing native networks with purely synthetic exogenous circuits that route cell fate through precisely controlled ectopic expression of pathway regulators provides a less invasive scheme for directing cell fate. Such control systems require little or no manipulation of the host's native genetic material, preserve access to wild-type behaviors, and minimize difficulty in transfer to higher eukaryotes. Modulation of pathway components at key control points, or pathway regulators, can alter a network response and redirect cellular fate. Introducing feedback loops at these control points reshapes network topology, alters dynamic signaling profiles, and may enhance robustness of phenotypic selection (*22*, *23*). Synthetic RNA-based transducers can be used to link diverse environmental signals to exogenous control systems so as to reshape network topology conditionally and to redirect cell fate (*4*, *5*, *24*). These synthetic control systems, or molecular network diverters, are composed of a promoter, which acts as a modulator; a pathway regulator; and an RNA-based transducer (Fig. 1, A and B). The modulator and transducer determine the strength, mode, and signal responsiveness of a diverter. Molecular network diverters conditionally divert the native network and confer orthogonal control of cell fate within a genetically homogenous cell population through specified environmental signals. Orthogonal control through diverters provides an added degree of freedom in specifying cell fate, as it preserves existing mechanical, chemical, and biochemical channels. We set out to develop molecular network diverters to activate or attenuate signaling through a native MAPK pathway to conditionally redirect, or route, cells to one of three distinct fates.

Results

Identifying Control Points Within Natural Networks

To build molecular network diverters for the yeast mating pathway, we identified titratable positive and negative regulators of pathway activity that result in divergent cell fate decisions when ectopically expressed (Fig. 1C). We measured pathway activity by monitoring fluorescence from a transcriptional reporter combined with green fluorescent protein (*pFUS1-GFP*). Cell fate determination was measured through halo assays, where cells are plated around a filter disc saturated in pheromone. The disc creates a pheromone concentration gradient, and mating-associated cell cycle arrest above a certain concentration of pheromone from wild-type cells results in a "halo" or cleared region around the disc. We used an engineered galactose-inducible promoter system to titrate amounts of various pathway signaling proteins (*25*). The set of tested pathway proteins was selected for those that were more likely to dominate pathway activity and to exhibit minimal toxicity when overexpressed (*26*, *27*). The majority of examined proteins failed to alter pathway activation when overexpressed, which supported the hypothesis that, within native pathways, regulatory architectures filter out perturbations in the amounts of various components (*28*–*34*). Despite the endogenous control schemes, we identified two control points where ectopic overexpression of associated signaling proteins dominated pathway activity (Fig. 2, A and B, and fig. S1, A and B). Ste4 activated the mating pathway and induced cell cycle arrest in the absence of pheromone (fig. S2A), whereas overexpression of Msg5 reduced pathway activation and eliminated pheromone-induced cell cycle arrest (fig. S2B).

We examined the relations between pathway response and the predicted abundance of the regulator (Ste4 or Msg5). Amounts of each pathway regulator were varied by pairing the regulator with promoters and RNA-based transducers of various activities (Fig. 2, C, D, and E). By compiling pathway activity data, we determined the pathway response curve as a function of predicted Ste4 concentrations, calculated from the combined promoter and transducer activities (Fig. 2F, fig. S3, and supplementary text S1). By combining the pathway response curve with data on cell fate, we identified a narrow transitory range of ectopic Ste4 expression at which cell fate diverged from wild-type to an alternative "mating" fate. The "mating" fate is characterized by constitutive activation of the pathway and cell cycle arrest in the absence of pheromone, which results in undetectable cell growth outside the halo region. We also examined a positive-feedback architecture by replacing the constitutive promoter (*pC*) with

[1]Division of Chemistry and Chemical Engineering, 1200 East California Boulevard, MC 210-41, California Institute of Technology, Pasadena, CA 91125, USA. [2]Department of Mechanical Engineering, 900 University Avenue, University of California at Riverside, Riverside, CA 92521, USA. [3]Department of Bioengineering, 473 Via Ortega, MC 4201, Stanford University, Stanford, CA 94305, USA.

*Corresponding author. E-mail: csmolke@stanford.edu

the pathway-responsive promoter (*pFB*), which increased expression of the regulator in response to pathway activity. To analyze the quantitative effect of the various modes of expression (*pC*, *pFB*) on the pathway response to Ste4, we fit each response curve to a Hill function (table S1). The Hill function model indicates that the positive-feedback architecture shifted the concentration of Ste4 at which half-maximal pathway activation (EC_{50}) was achieved to predicted concentrations of Ste4 almost 1/10th those for the nonfeedback system ($EC_{50\text{-}Ste4,FB}$ = 0.02, $EC_{50\text{-}Ste4,C}$ = 0.21) (Fig. 2F). The results support the hypothesis that positive feedback increased the pathway sensitivity to Ste4 expression, which shifted the threshold of pathway response to lower amounts of Ste4 and sharpened the divergence of the wild-type and mating fates.

Using similar strategies, we generated pathway response curves as a function of predicted concentrations of the negative regulator, Msg5, under constitutive (*pC*) and feedback (*pFB*) expression. Quantification of the pathway response characteristics was performed by fitting the data to a Hill function (table S2). In contrast to the Ste4 system, the Msg5 systems demonstrated different efficacies ($V_{max\text{-}Msg5,C}$ = 0.86, $V_{max\text{-}Msg5,FB}$ = 0.53), which resulted in different maximal pathway attenuation for each expression mode (*pC* or *pFB*) (Fig. 2G). Constitutive expression of Msg5 resulted in a sharper decrease in pathway activity and greater maximal pathway attenuation compared with the negative-feedback architecture, which showed a more graded response that leveled out to higher values of pathway activity. For both modes of Msg5 expression, the pathway response curves combined with the phenotypic assays demonstrated a low and narrow range of ectopic Msg5 expression (<0.1) across which cell fate diverged from wild-type to an alternative "nonmating" fate. The "nonmating" fate is characterized by constitutive inhibition of the pathway and cell cycle arrest in the presence of pheromone, which resulted in cell growth into the halo region. The data indicate that Msg5 is a potent regulator of pathway activity.

Developing Positive and Negative Diverters Based on Identified Control Points

We constructed a positive diverter with a positive-feedback architecture to activate the pathway in the absence of pheromone in response to an environmental signal. By using the pathway-responsive promoter (*pFB*) and various tetracycline-responsive RNA-based transducers (*SXtc*) to control Ste4 expression, we constructed positive-feedback diverters of varying strength. Within the positive-feedback architecture (*pFB-Ste4-SXtc*), we identified transducers that demonstrated robust small-molecule pathway activation and routing of cells to the mating fate (Fig. 3A and fig. S1C). As transducer activity increased, and thus increased the strength of the positive-feedback diverter, cells exhibited increasing pathway activity. Positive-feedback diverters composed of tetracycline-responsive transducers S3tc and S4tc activated the mating pathway and induced switching to the mating fate in the presence of tetracycline while maintaining the wild-type fate in its absence, as measured by halo assays. We also constructed positive diverters without feedback (*pC-Ste4-SXtc*) with the same components as the positive-feedback diverters except with a constitutive promoter (*pC*) replacing the pathway-responsive promoter. As expected from the pathway response curves (Fig. 2F), the positive diverters without feedback, or booster diverters, exhibited weaker effects than the positive-feedback diverters (fig. S4). We built positive diverters with and without feedback (*pFB-Ste4-SXth* and *pC-Ste4-SXth*) with theophylline-responsive RNA-based transducers (*SXth*), which allowed similar control of cell fate with a different small-molecule input (fig. S5). Transducers responsive to different inputs with similar basal activities and dynamic ranges induced similar pathway activities and similarly routed cells to the mating fate, which indicated that fate routing is independent of the input signal identity. The data support the ability to rationally tune network diverters through the exchange of modular, well-defined parts.

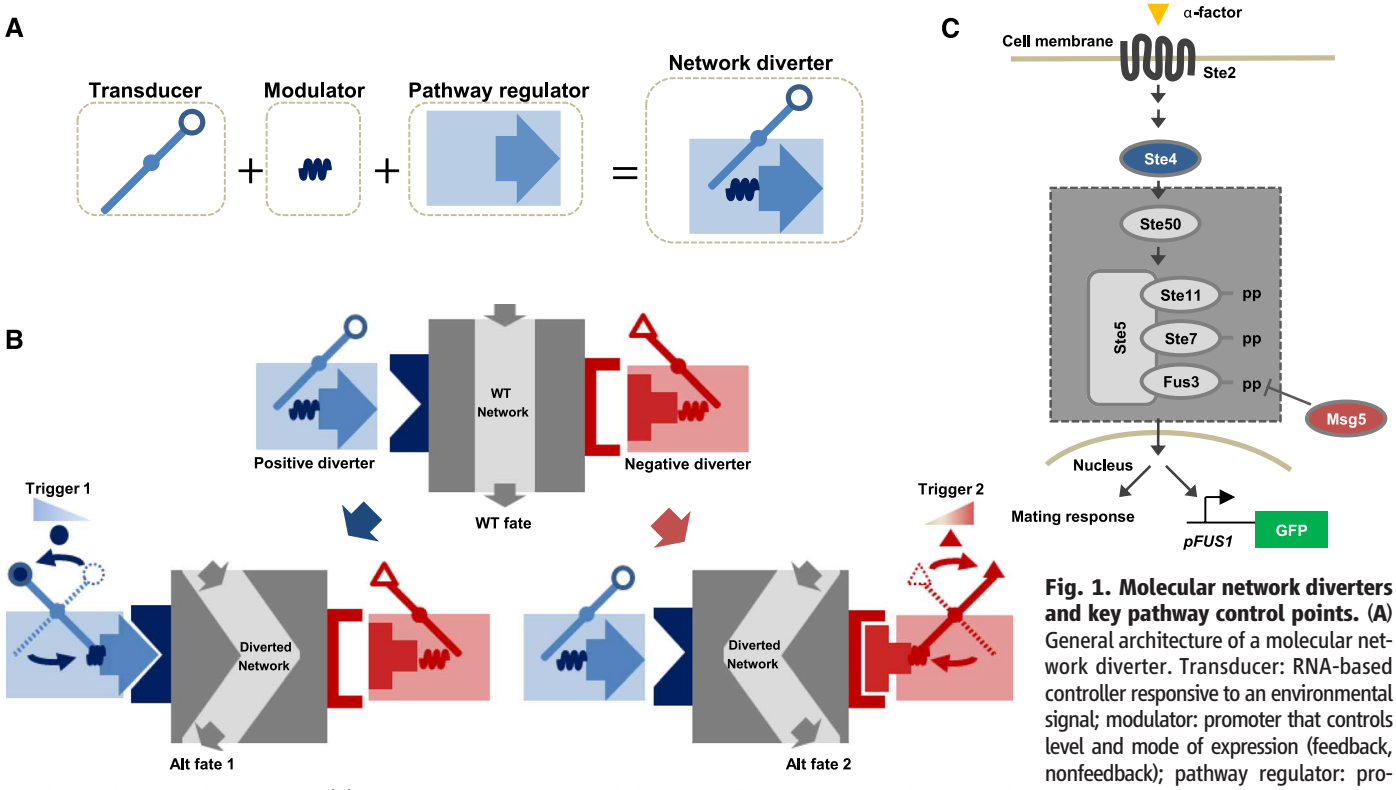

Fig. 1. Molecular network diverters and key pathway control points. (**A**) General architecture of a molecular network diverter. Transducer: RNA-based controller responsive to an environmental signal; modulator: promoter that controls level and mode of expression (feedback, nonfeedback); pathway regulator: protein that modulates pathway activity. (**B**) Diagram of molecular network diverters reshaping native signaling networks in response to environmental signals. WT, wild type. (**C**) Schematic of the yeast mating pathway. Pheromone (α-factor) binds to a transmembrane receptor (Ste2), where the signal is relayed through G proteins (Ste4), an adaptor protein (Ste50), and a scaffold-bound (Ste5-bound) three-tiered MAPK cascade. Phosphorylated Fus3 (dephosphorylated by Msg5) is translocated to the nucleus, which results in activation of mating genes. Pathway activity and mating response are monitored through a *pFUS1-GFP* reporter and pheromone-induced cell cycle arrest, respectively.

We constructed negative diverters to attenuate the pathway in the presence of pheromone in response to an environmental signal using similar design strategies. Because of the efficacy and potency of Msg5, negative diverters that maintained wild-type fate in the absence of input signal required stringent transducers (those with low basal activities) (*35*). We evaluated pathway attenuation and fate routing by negative diverters

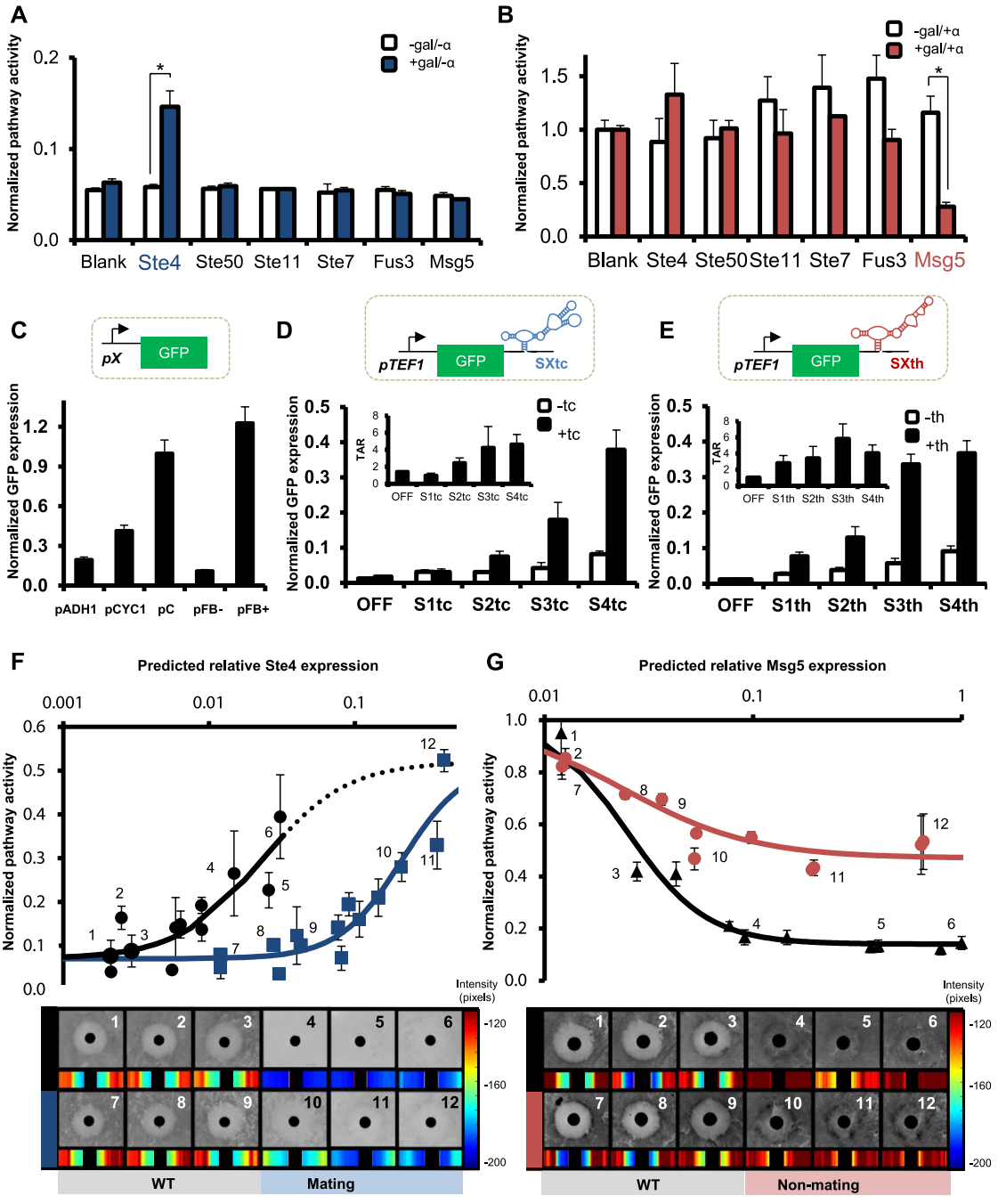

Fig. 2. A synthetic biology toolbox for constructing molecular network diverters. (**A**) Identification of activating regulators. Normalized pathway activity is reported as the geometric mean GFP value from cells overexpressing (+gal) or not overexpressing (-gal) the indicated proteins of the mating pathway. GFP values are normalized to that of the control (cells harboring a blank plasmid in the presence of saturating pheromone at the corresponding galactose concentration; gal: -gal, no galactose; +gal, 1% galactose; α: -α, no α mating factor; +α, 100 nM α mating factor). For $n = 3$, $^*P < 0.01$. (**B**) Identification of attenuating regulators. Normalized pathway activity from attenuating constructs is reported as described in (A) except that cells were assayed in the presence of saturating concentration of pheromone. (**C**) Relative promoter activities for modulating concentrations of pathway regulators. Three constitutive promoters (*pADH1*, *pCYC1*, and *pTEF1mutant7/pC*) and one mating-responsive promoter (*pFUS1/pFB*) were characterized. *pFB* activities were measured in the absence (pFB-) and presence (pFB+) of α-factor. Normalized GFP expression is reported as the geometric mean GFP value from cells harboring the specified construct normalized to that of the control (cells harboring the *pC* construct). (**D** and **E**) Activities of tetracycline-responsive (SXtc) (D) and theophylline-responsive (SXth) (E) RNA transducer sets (th: -th, no theophylline; +th, 5 mM theophylline; tc: -tc, no tetracycline; +tc, 1 mM tetracycline). Normalized GFP expression is reported as the geometric mean GFP value from cells harboring the specified construct normalized to that of the control (cells harboring the ON state control construct at the corresponding signal concentration). The TAR (transducer activation ratio) is reported as the ratio of normalized GFP expression for a given transducer in the presence and absence of signal. For $n \geq 3$, $P < 0.001$ for all noncontrol transducers. (**F**) Pathway response as a function of predicted Ste4 expression for constitutive and feedback architectures (circles: *pFB*; squares: *pC*). Predicted relative Ste4/Msg5 expression is reported as the calculated expression normalized to that of the control (construct pairing *pC* and ON RNA transducer). Normalized pathway activity from activating constructs is reported as the geometric mean GFP value from cells harboring the specified construct in the absence of pheromone at the indicated signal concentration normalized to that of the control (cells harboring a blank plasmid in the presence of saturating pheromone). Each data set is fit to a Hill function (line). Dash indicates extrapolated fit. Numbers indicate corresponding pathway activity and cell cycle arrest data for identical constructs. (**G**) Pathway response as a function of predicted Msg5 expression for constitutive and feedback architectures (triangles: *pC*; circles: *pFB*). Normalized pathway activity from attenuating constructs is reported as described in (F) except that cells are assayed in the presence of saturating pheromone. Values reported represent means ± SD for $n \geq 3$.

with the constitutive architecture and theophylline-responsive transducers (*pC-Msg5-SXth*) (Fig. 3B and fig. S1D). Pathway activity decreased with increasing transducer activity and maintenance of the wild-type halo in the absence of theophylline required stringent transducers (S1th, S2th) (Fig. 2E). The negative diverter without feedback, or resistance diverter, composed of theophylline-responsive transducer S2th reduced mating pathway activity and induced switching to the nonmating fate in the presence of theophylline while maintaining a slightly diminished wild-type fate in its absence. Fate routing was not observed with any single negative diverter constructed with the feedback architecture (*pFB-Msg5-SXth*), although cells harboring individual constructs within the negative-feedback set adopted either wild-type or nonmating fates (fig. S6). The Hill function model of the pathway response to negative feedback indicates that this architecture has reduced efficacy (Fig. 2G). The data indicate that the pathway is less sensitive to negative feedback (*36*). Thus, the transducers do not span the requisite expression range separating the wild-type and nonmating fates in this architecture. Reduced pathway sensitivity to changes in Msg5 concentrations would be expected to result in smaller changes in pathway activity, which could prevent fate routing.

Dual Diverter Highlights Need to Precisely Balance Opposing Activities

A dual diverter is a genetic control system that will support routing of an entire cell population to one of three cell fates in response to specified environmental signals. We designed a dual-diverter architecture that integrated positive and negative diverters optimized for independent cell fate routing to either the mating or nonmating fates. We paired several tetracycline-responsive positive-feedback diverters (*pFB-Ste4-SXtc*) with resistance diverters that incorporated a set of theophylline-responsive RNA transducers (*pC-Msg5-SXth*) to examine effects of pairing diverters encoding opposing functions. When opposing diverters that route signals through a native network are integrated, basal activity from the nontriggered diverter may antagonize routing from the triggered diverter (Fig. 4A), even if, independently, neither diverter affects cell fate in the absence of their cognate signal. Our results indicate that integrating the independently optimized positive-feedback and resistance diverters leads to antagonism, such that independent routing to the alternative fates cannot be achieved in cells harboring these opposing functions (fig. S7).

We developed a simple black-box model of our system to explore the pathway response to integration of multiple modules (i.e., individual regulator expression cassettes such as positive-feedback, booster, negative-feedback, and resistance modules) of varying strength set by transducer activity (Fig. 4B and table S3). We analyzed the dual-diverter architecture that integrated positive-feedback and resistance diverters by simulating pathway output for varying positive-feedback and resistance strengths in the absence and presence of pheromone (Fig. 4C). The model predicts that pathway activation across the range of positive-feedback strengths was significantly diminished even in the presence of a low-strength resistance diverter and completely inhibited for resistance strengths (amounts of Msg5) above $K_{M,Msg5}$ (the concentration of Msg5 at which half-maximal pathway attenuation was achieved). The modeling results suggest that, even at a resistance strength corresponding to the lowest basal transducer activity, the resistance module will inhibit pathway activation from the positive-feedback diverter.

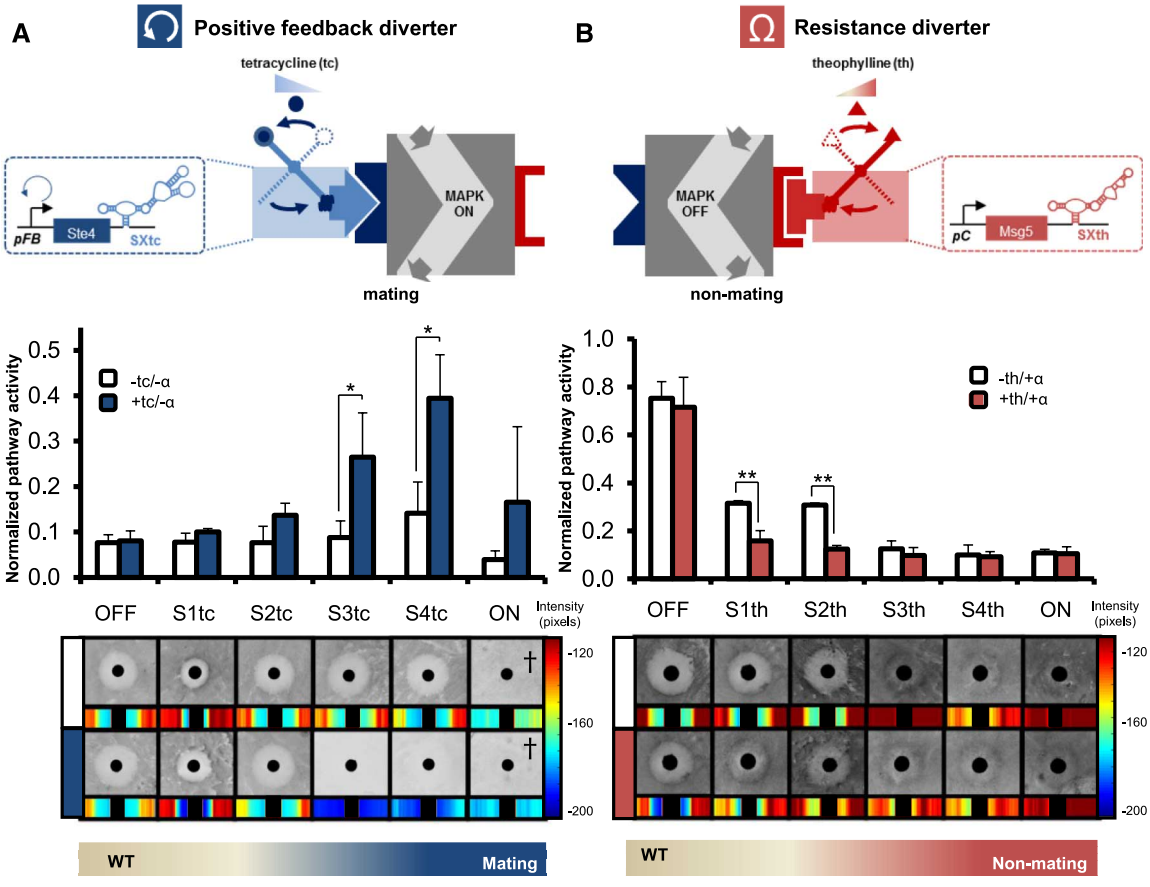

Fig. 3. Optimized design of independent positive and negative diverters. (**A**) A positive-feedback diverter supports robust pathway activation in the absence of pheromone (-α) and cell fate routing to the mating fate (tc: -tc, no tetracycline; +tc, 1 mM tetracycline). Normalized pathway activity from activating constructs is reported as described in Fig. 2F. Dagger: see fig. S3 and supplementary text S1. (**B**) A resistance diverter supports robust pathway attenuation in the presence of pheromone (+α) and cell fate routing to the nonmating fate (th: -th, no theophylline; +th, 5 mM theophylline). Normalized pathway activity from attenuating constructs is reported as described in Fig. 2G. For $n \geq 5$, $^{*}P < 0.05$, $^{**}P < 0.005$. Values reported represent means ± SD.

Conversely, positive-feedback strength limited the maximal attenuation from the resistance diverter, which led to reduced maximal attenuation as positive-feedback strength increased. These results indicate that the basal expression from the integrated opposing diverters may significantly antagonize the other diverter.

Given the limitations of performance for a dual diverter based on integrating the positive-feedback and resistance diverters, we examined alternative designs to limit antagonism and enhance the cell fate–routing functions. The modeling results indicate that strategies based on modifying the strength of the positive-feedback diverter for increased activity may limit the performance of the negative diverter (Fig. 4C). Thus, we used the model to examine the impact of adding a second positive module, or a booster module encoding constitutive expression of Ste4, to the positive-feedback diverter (Fig. 4D). The combination of the booster and positive-feedback modules enhanced system tolerance to Msg5 expression and allowed for pathway activation at amounts of Msg5 produced at basal strength (in the absence of cognate signal) of the resistance diverter. In the absence of its cognate signal, the basal strength of the booster module was predicted to have minimal effect on attenuation from the resistance diverter.

Based on the enhancement to the performance of the positive diverter achieved by combining two modules, we examined the impact of adding a second negative module, or a negative-feedback module, to the resistance diverter (Fig. 4E). Negative feedback was predicted to globally enhance attenuation and to make it robust to minor variations in Ste4 and Msg5 expression from the other modules. The addition of negative feedback to the negative diverter was predicted to have minimal impact on pathway activation

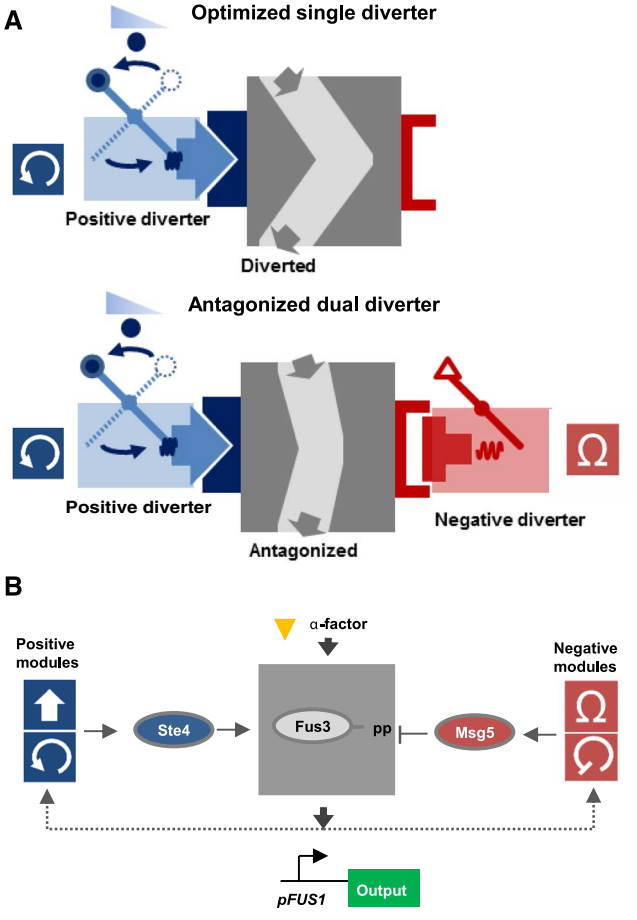

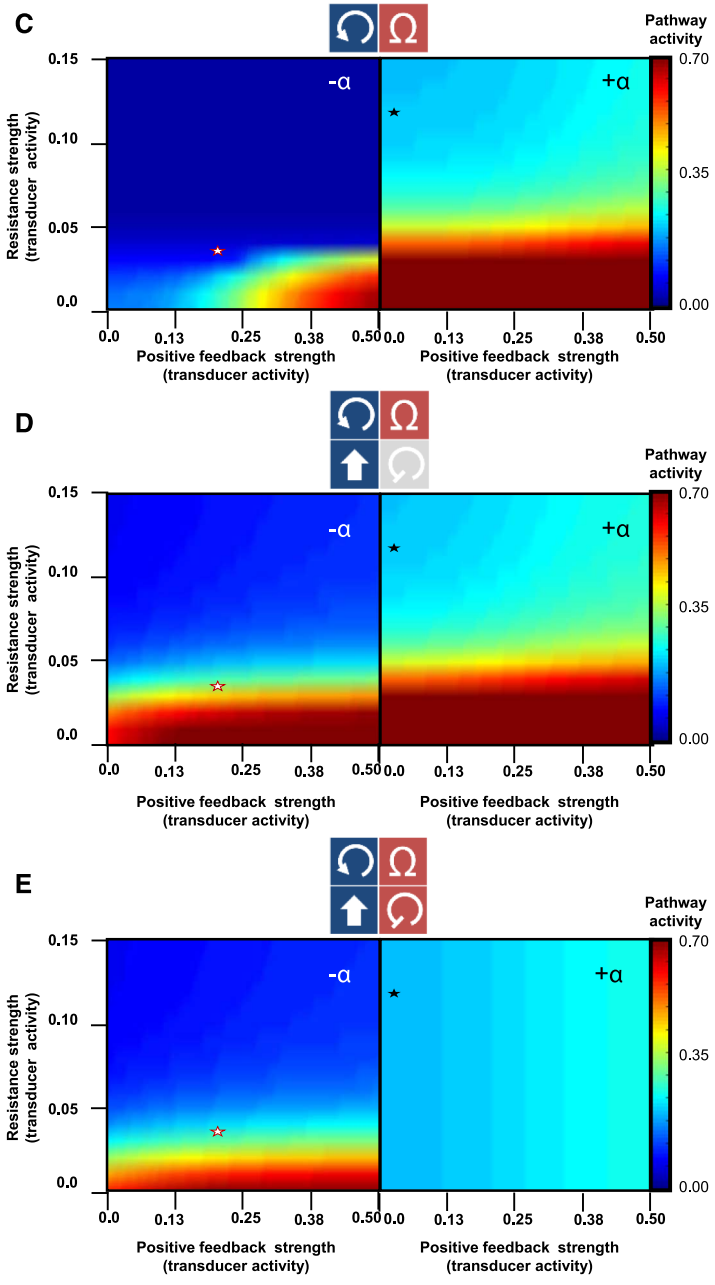

Fig. 4. Integration of opposing diverters optimized for independent cell-fate routing results in antagonism. (**A**) Diagram of the integration of independently optimized opposing diverters resulting in antagonism, which inhibits the diverters from routing cells to alternate fates. (**B**) Schematic of black-box model of system with native pheromone input and synthetic Ste4 and Msg5 input to active Fus3 with *pFUS1* activity as the model output. (**C** to **E**) Model of pathway activation in the absence of pheromone (left, -α) and attenuation in the presence of pheromone (right, +α) as a function of varying strengths of the positive-feedback and resistance diverters. To represent the presence or absence of cognate signals for each diverter, simulations were performed with booster strength set to 0 (C), S4tc (+tc: 0.41, left, D and E), and S4tc (-tc: 0.08, right, D and E); negative-feedback strength set to 0 (C and D), S3th (-th: 0.06, left, E), and S3th (+th: 0.34, right, E). White star: positive-feedback strength: S3tc (+tc: 0.21); resistance strength: S2th (-th: 0.04). Black star: positive-feedback strength: S3tc (-tc: 0.04); resistance strength: S2th (+th: 0.13).

through the positive diverter. Thus, the model predicts that restructuring the positive and negative diverters to include two differentially regulated modules of the same pathway regulator will enhance the function of the individual diverters, while minimizing the impact on the opposing diverter.

Genetic Strategies for Minimizing Pathway Antagonism

We developed and incorporated a number of strategies to reduce antagonism in the dual diverter and to allow for routing to multiple fates. We constructed an alternative RNA transducer architecture that minimized basal expression from the positive-feedback diverter in response to the cognate signal from the negative diverter to maximize pathway attenuation. The composite transducer S3tc—comprising S4tc (tetracycline-responsive "ON" switch) and S1OFFth (theophylline-responsive "OFF" switch)—was designed to reduce expression of Ste4 in response to theophylline and to increase Ste4 expression in response to tetracycline (Fig. 5A). When this composite transducer was implemented in the positive-feedback diverter, pathway activity was between those of S2tc and S4tc for basal and tetracycline-triggered activities. In the presence of theophylline, activity for S3tc was similar to S2tc basal activity (Fig. 5B). Thus, S3tc yielded a larger fold difference in pathway activity (8.0; $activity_{tc}$: $activity_{th}$) than did S2tc (3.8) or S4tc (2.5). Several integrated dual-diverter configurations that used the positive-feedback diverter incorporating S3tc (*pFB-Ste4-S3tc*) achieved strong pathway attenuation when paired with resistance diverters. As predicted from the model, all configurations displayed weak pathway activation (fig. S8), which suggested that basal expression of Msg5 from the resistance diverter prevented the requisite pathway activation to trigger positive feedback–induced amplification. Improved performance of a dual diverter may be achieved with the use of RNA transducers exhibiting even lower basal activities and larger dynamic ranges. However, computational models of RNA transducer activities indicate a trade-off between stringency and input sensitivity of these genetic devices (*37*). Given these constraints, the dual-diverter architecture is inherently biased to allow basal expression from the opposing diverters to promote antagonism, which cannot be mitigated solely by changing transducer or promoter activities.

We developed an alternate positive-diverter architecture to support increased pathway activation with minimal impact on the negative diverter (Fig. 5C). The modeling results indicate that strategies based on modifying the strength of the positive-feedback module for increased activity limit the performance of the negative diverter (Fig. 4C). Thus, we added a second module, or a booster module, encoding constitutive expression of Ste4 and a strong tetracycline-responsive RNA-based transducer (*pC-Ste4-S4tc*), to the positive-feedback diverter. The resulting enhanced positive diverter, or amplifying diverter, combined a positive-feedback module (*pFB-Ste4-S3tc*) and booster module (*pC-Ste4-S4tc*) to increase pathway activation while minimizing antagonism of the attenuating function of the negative diverter. As predicted by the model, this dual-diverter architecture restores pathway activation (Fig. 5E). However, this architecture did not allow for routing to the nonmating fate (fig. S9). The data indicate that amplification of pathway activation from the positive-feedback module in the amplifying diverter in the presence of high concentrations of pheromone overwhelmed attenuation from the resistance diverter.

To counteract amplification from the amplifying diverter at high concentrations of pheromone, we constructed an enhanced negative diverter by adding a negative-feedback module, linking a pathway-responsive promoter and a theophylline-responsive RNA-based transducer to Msg5 (*pFB-Msg5-SXth*) to the resistance diverter (Fig. 5D). The resulting attenuating diverter combined a negative-feedback module (*pFB-Msg5-S3th*) and resistance module (*pC-Msg5-S2th*) (Fig. 5D). As predicted by the model, the attenuating diverter had minimal impact on pathway activation through the amplifying diverter, which retained tetracycline-induced routing to the mating fate (Fig. 5E).

We observed that the robustness of pathway activation varied with the different dual-diverter architectures. Although effective in routing cells to the mating fate, the high basal pathway activity associated with the positive-feedback diverter provided little resolution between triggered and nontriggered populations (Fig. 5E and fig. S10A). Addition of the resistance diverter inhibited routing to the mating fate. By combining the positive-feedback and booster modules in the amplifying diverter, cells were routed to the mating fate in the presence of the resistance diverter. Addition of the negative-feedback module significantly increased resolution by reducing population heterogeneity (fig. S10B).

We probed the performance of the dual diverter constructed with amplifying and attenuating diverters under varying strengths of the resistance module by varying the transducer activity (*pC-Msg5-SXth*). The data demonstrated a strong correlation between resistance strength and pathway activity (Fig. 5F). Pathway activation diminished and attenuation increased with increasing resistance strength (fig. S11, A and B). Thus, resistance strength must be precisely tuned for the dual diverter to achieve routing to multiple alternative and divergent cell fates.

We used our model to analyze the impact of the resistance module on system robustness and output. Basal concentration of Msg5 from the resistance module acts as a buffer to pathway activity, by filtering out perturbations in Ste4 concentrations from the amplifying diverter (Fig. 5G). In the presence of the resistance module, the amplifying diverter maintains low pathway activity until Ste4 concentrations cross a threshold and pathway activity is amplified. We evaluated the buffer capacity of the system by identifying the Ste4 expression from the booster module that resulted in pathway activation (above basal pathway activity ~0.07) as a function of resistance strength (Fig. 5H). Buffer capacity increased for increasing resistance strength and was inversely related to pathway activation with an optimum for buffer capacity and pathway activation when resistance strength is set at 80% of $K_{M,Msg5}$. Our results suggest that there is a trade-off in tuning our system for both signal output and robustness.

Optimized Dual Diverter Routes Cells to Three Distinct Fates

Our optimized dual diverter integrated a number of strategies to minimize antagonism, including improved transducer architecture, amplifying and attenuating diverters, and a precisely tuned amount of resistance (Fig. 6, A and B). Although the dual diverter (booster: *pC-Ste4-S4tc*; positive feedback: *pFB-Ste4-S3tc;* resistance: *pC-Msg5-S2th;* negative feedback: *pFB-Msg5-S3th*) exhibited lower pathway activation than did the positive-feedback diverter alone or ON control (dual diverter without the negative-feedback module), the dual diverter exhibited a stronger fold pathway activation (7.2) than the positive-feedback diverter (1.6), approaching that of the ON control (10.9) (Fig. 6C). The dual-diverter attenuated pathway activity as well as the resistance diverter alone, and the pathway activity approached that of the OFF control (positive feedback: *pFB-Ste4-OFF*; resistance: *pC-Msg5-S3th*; negative feedback: *pFB-Msg5-S3th*) (Fig. 6E). The dual diverter routed cells to the mating fate as well as did the positive-feedback diverter (Fig. 6D). Additionally, the cells harboring the dual diverter maintained a more robust wild-type halo compared with those harboring the resistance diverter, while routing nearly as well to the nonmating fate. Finally, cell routing could be modulated through the concentration of environmental signals (fig. S11C). Although the ON control and dual diverter exhibited similar pathway attenuation, only the latter routed cells to the nonmating fate, which indicated that negative feedback is a critical element in regulating longer time-scale events, such as cell cycle arrest. Thus, the optimized dual diverter achieved conditional routing of genetically identical cells to diverse phenotypes in response to distinct molecular signals.

Beyond controlling transcriptional activation of the pathway and cell cycle arrest, the diverters also controlled mating. The positive-feedback diverter and the ON control allowed a tetracycline-induced increase in mating efficiency and increased basal mating efficiency (Fig. 6F). The resistance diverter and the OFF control exhibited a theophylline-triggered reduction in mating efficiency. The dual diverter increased mating efficiency by ~70% in response to tetracycline, similar to the effect of the positive-feedback diverter (~66%), and reduced mating efficiency to an amount similar to that from cells harboring the resistance diverter in the presence of theophylline. The mating data indicated that the dual diverter is

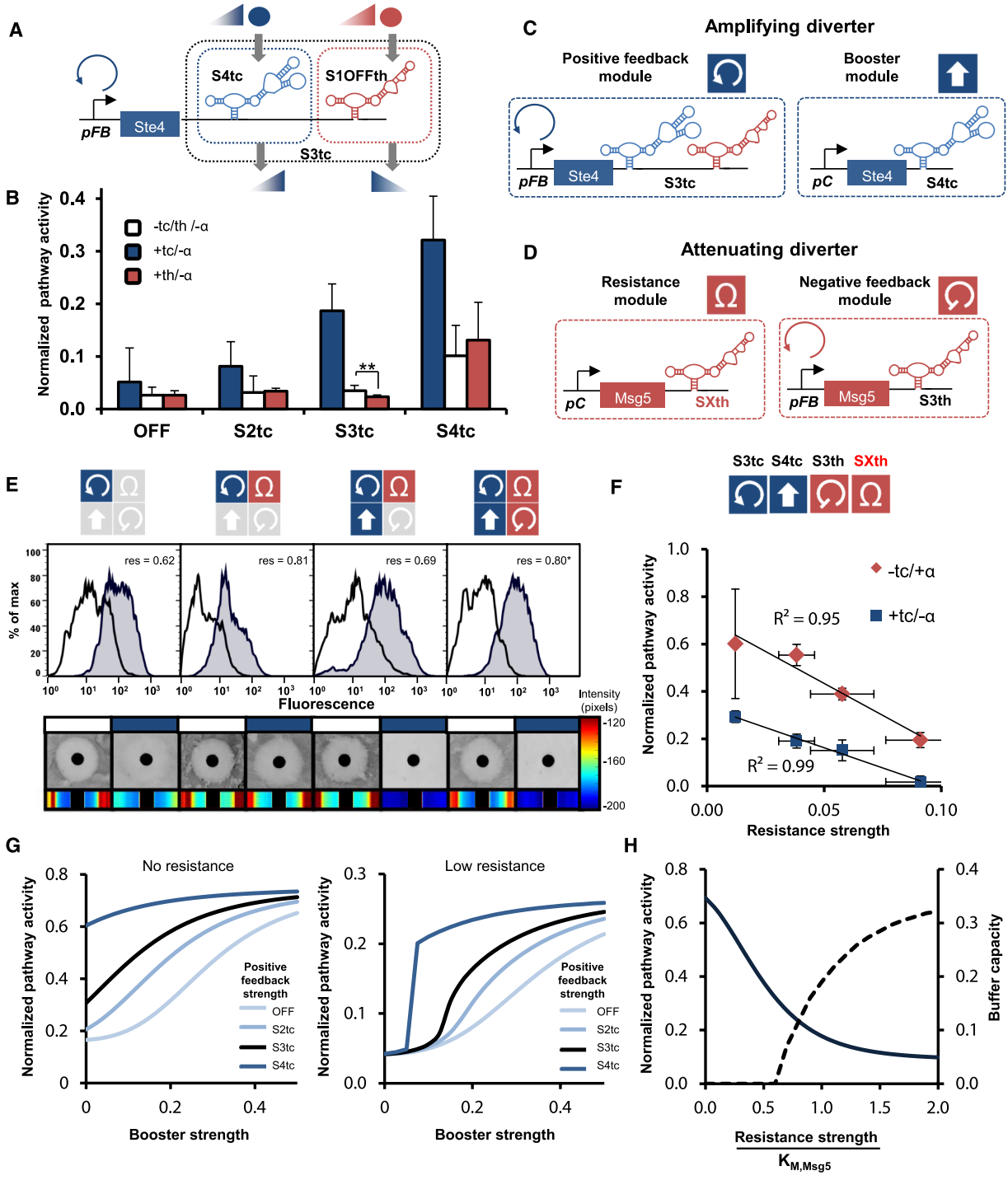

Fig. 5. Optimizing the dual-diverter architecture and components for the integration of opposing diverters. (**A**) Schematic of the composite RNA transducer S3tc designed to reduce expression of the linked regulator in response to theophylline and increase expression in response to tetracycline. (**B**) Pathway activity of cells with composite transducer S3tc in response to tetracycline or theophylline (tc: -tc, no tetracycline; +tc, 1 mM tetracycline; th: -th, no theophylline; +th, 20 mM theophylline; α: -α, no α mating factor; +α, 100 nM α mating factor). For $n = 6$, $^{**}P < 0.02$. (**C**) Schematic of the amplifying diverter comprising a positive-feedback module and a booster module. (**D**) Schematic of the attenuating diverter comprising a resistance module and a negative-feedback module. (**E**) Impact of resistance, booster, and negative-feedback modules on the resolution and variation in population-level pathway activation and routing to mating fate for cells harboring the positive-feedback module (white: 0 mM tetracycline; blue: 1 mM tetracycline). GFP histograms for triggered and nontriggered cell populations and routing to the mating fate are shown for cells harboring: (left) the positive-feedback module (*pFB-Ste4-S3tc*); (second from left) the positive-feedback and resistance (*pC-Msg5-S2th*) modules; (second from right) the positive-feedback, resistance, and booster (*pC-Ste4-S4tc*) modules; (right) the positive-feedback, resistance, booster, and negative-feedback (*pFB-Msg5-S3th*) modules. For $n = 3$, $^{*}P < 0.0005$. (**F**) Pathway activity of the dual diverter as a function of varying resistance strength. R^2 represented for linear fit of data. (**G**) Predicted pathway activation from the dual diverter as a function of booster strength in the absence (left) and presence (right) of low resistance. Lines represent predicted relations under the indicated positive-feedback strengths, as set by transducer activity. (**H**) Predicted pathway activation and buffer capacity from the dual diverter as a function of varying resistance strength relative to $K_{M,Msg5}$. Solid: pathway activity; dashed: buffer capacity. Values reported represent means ± SD for $n \geq 3$.

optimized to route cells to the divergent fates as effectively as each single diverter.

Discussion

Our studies describe a class of genetic control systems, molecular network diverters, that route cells to divergent fates in response to specified environmental signals. The system integrates complex positive and negative routing functions through stringent RNA-based transducers to limit antagonism, amplify activation, and induce attenuation, which allows genetically identical cells to be conditionally routed to one of three fates in response to specified environmental signals. We focused our analysis of the effects of the molecular network diverters on steady-state pathway activation, as measured by transcriptional activation of the pathway, and cell fate determination, as measured by cell cycle arrest and mating efficiency. Other properties of the network, including temporal response of pathway activation and pathway sensitivity to pheromone concentrations, can also be measured and analyzed for changes in the engineered systems and the relation of these network properties to fine-tuning cell fate decisions (*33*, *38*). Positive- or negative-feedback loops, as well as constitutive overexpression of signaling components, can tune MAPK pathways for prescribed temporal pathway activation responses (*19*). In addition, altering the

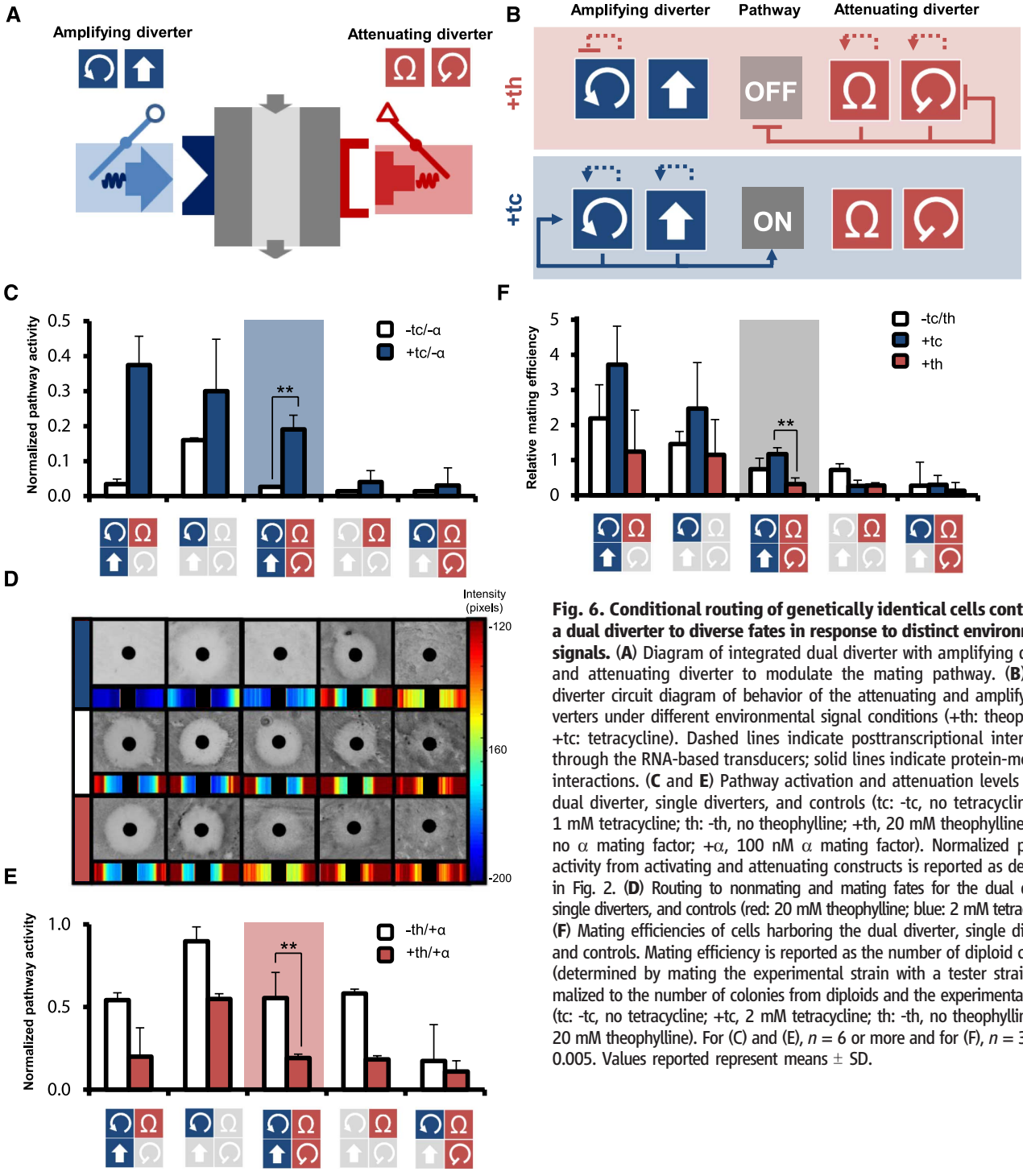

Fig. 6. Conditional routing of genetically identical cells containing a dual diverter to diverse fates in response to distinct environmental signals. (**A**) Diagram of integrated dual diverter with amplifying diverter and attenuating diverter to modulate the mating pathway. (**B**) Dual-diverter circuit diagram of behavior of the attenuating and amplifying diverters under different environmental signal conditions (+th: theophylline; +tc: tetracycline). Dashed lines indicate posttranscriptional interactions through the RNA-based transducers; solid lines indicate protein-mediated interactions. (**C** and **E**) Pathway activation and attenuation levels for the dual diverter, single diverters, and controls (tc: -tc, no tetracycline; +tc, 1 mM tetracycline; th: -th, no theophylline; +th, 20 mM theophylline; α: -α, no α mating factor; +α, 100 nM α mating factor). Normalized pathway activity from activating and attenuating constructs is reported as described in Fig. 2. (**D**) Routing to nonmating and mating fates for the dual diverter, single diverters, and controls (red: 20 mM theophylline; blue: 2 mM tetracycline). (**F**) Mating efficiencies of cells harboring the dual diverter, single diverters, and controls. Mating efficiency is reported as the number of diploid colonies (determined by mating the experimental strain with a tester strain) normalized to the number of colonies from diploids and the experimental strain. (tc: -tc, no tetracycline; +tc, 2 mM tetracycline; th: -th, no theophylline; +th, 20 mM theophylline). For (C) and (E), $n = 6$ or more and for (F), $n = 3$, $^{**}P < 0.005$. Values reported represent means ± SD.

relative amounts of pathway kinases can tune the sensitivity of the pathway response to pheromone concentrations (*33*). Thus, the molecular network diverters can be adapted to the regulation of other pathway signaling components to engineer a wider range of network properties.

The modular architecture of the diverters, availability of tuned RNA-based transducers, and incorporation of feedback allow for precise balancing of positive and negative regulator activities even in the presence of external pathway stimulation. Our work identified design principles for networks that induce differentiation of cells in response to environmental signals and that enhance the robust performance of integrated mutually antagonistic genetic programs. As an example, integrated negative regulators can act to buffer a system to noise amplification mediated through positive-feedback loops by providing a resistance to amplification. Additionally, pathway output can be tuned through resistance, which may be a key design consideration when adopting the network diverter architecture to new signaling pathways with different thresholds of pathway activity corresponding to alternative fates. Further, negative feedback can play an important role by reducing population heterogeneity and mediating robust, long-term cell fate decisions. The dual-diverter configuration enables routing to alternative fates and minimizes impact on the opposing diverter by integrating differential regulatory strategies on functionally redundant genes. Differential regulation of functionally redundant parts is observed in natural biological networks, such as those regulating bone formation, osteoblast differentiation, plant defense, and metabolism (*39*, *40*), and may represent a common strategy for amplifying and attenuating pathway responses to environmental signals.

Our studies focused on the development and elucidation of design principles for this class of genetic control systems in the model organism *S. cerevisiae*. Conservation of the form and function of MAPK pathways through higher eukaryotes highlights the possible applications of these controllers in mammalian systems. For example, a threefold overexpression of MPK-1 (homolog to yeast Msg5) can significantly reduce MAPK phosphorylation and block persistent pathway activation (*41*). In addition, overexpression of MPK-1 blocks apoptosis by inhibiting extracellular signal-regulated kinase and c-Jun N-terminal kinase signaling (*42*–*44*). As another example, overexpression of a neuroendocrine-associated phosphatase can suppress nerve growth factor–stimulated neuron differentiation in PC12 cells (*45*). However, differences in the regulation of these pathways in higher organisms compared with yeast may prohibit a direct translation of the strategies described here, and extension into higher organism may require further engineering optimization efforts.

Molecular network diverters provide a foundation for robustly programming spatial and temporal control over cell fate. The extension of similar control strategies to mammalian systems may facilitate construction of sophisticated genetic programs encoding complex cellular functions, such as patterning of cell fate, tissue homeostasis, and autonomous immune surveillance (*14*). The connection of synthetic circuits to downstream effector processes, like drug-delivery and apoptosis, requires reliable signal processing to target therapeutic effects. Strategies that enhance the robustness of signal processing in synthetic circuits will enable such smart therapeutics. Our ability to construct synthetic circuits that interface with native pathways, like molecular network diverters, will continue to expand as more pathway-responsive genetic elements and regulatory RNAs are identified. Advances in our capabilities to extract information from and direct responses in native pathways will facilitate the translation of synthetic biology tools to applications in medicine and biotechnology.

Materials and Methods

Plasmid and Strain Construction

Details are available in Materials and Methods in the supplementary materials available online.

Measuring Promoter and RNA Transducer Activities

Details are available in supplementary materials.

Measuring Mating Pathway Activity Through a Transcriptional Reporter

For the galactose titration studies, plasmids harboring the galactose-inducible promoter (*pGAL1*) controlling expression of various pathway regulators (*STE4*, *STE50*, *STE11*, *STE7*, *FUS3*, and *MSG5*) and appropriate controls were transformed into the reporter yeast strain CSY532. Cells were inoculated into the appropriate dropout medium, grown overnight at 30°C, and backwards diluted into fresh medium in the presence of varying concentrations of galactose (0, 0.25, 0.5, 1, 2 and 3%) to an optical density at 600 nm (OD_{600}) of <0.1. To identify negative pathway regulators, after growing cells for 3 hours at 30°C, we stimulated them with saturating pheromone levels [100 nM final concentration of α mating factor (Sigma-Aldrich, St. Louis, MO)] to activate the mating pathway. The pathway was not stimulated when evaluating the potential of positive regulators. After 6 hours of growth after back-dilution, GFP fluorescence levels from the *pFUS1-yEGFP3* reporter were evaluated by flow cytometry using a Cell Lab Quanta SC flow cytometer (Beckman Coulter, Fullerton, CA). GFP was exited from a 488-nm laser, and emission was measured from 520/40-nm bandpass filter with a photomultiplier tube setting of 5.0. Cells were gated for viability on the basis of side scatter and electronic volume. For each sample, the GFP values of 10,000 viable cells were measured. Cells were then gated for GFP levels above background. Flow cytometry data were analyzed using the FlowJo v.10 (Tree Star, Inc.) software package. Normalized pathway activity is calculated as the geometric mean GFP value of cells harboring the indicated construct normalized to that of cells harboring the blank plasmid control (not bearing a gene) stimulated with saturating α mating factor at the corresponding galactose concentration for three biological replicates. Error bars represent the standard deviation of at least three replicates.

The molecular network diverter plasmids and appropriate controls were transformed into the reporter yeast strain CSY840. Cells were inoculated into the appropriate dropout medium, grown overnight at 30°C, and backwards diluted into fresh medium in the presence or absence of the appropriate trigger molecule (theophylline or tetracycline) at the specified concentration to an OD_{600} of <0.1. For negative diverters, after growing cells for 3 hours at 30°C, we stimulated cells with saturating pheromone levels (100 nM final concentration α mating factor) to activate the mating pathway, whereas we tested positive diverters in the absence of pheromone. After 6 hours of growth after back-dilution, GFP fluorescence levels from the *pFUS1-yEGFP3* reporter were evaluated by flow cytometry using a Cell Lab Quanta SC flow cytometer as described above. For cells stimulated with tetracycline, GFP values were corrected by subtracting the calculated tetracycline autofluorescence. Tetracycline autofluorescence was calculated as the difference in GFP values between the 0 mM and 1 mM tetracycline samples for the wild-type control. GFP values for the wild-type control were not altered in the presence of theophylline. Normalized pathway activity is calculated as the geometric mean GFP value of cells harboring the indicated construct normalized to that of cells harboring the blank plasmid control stimulated with saturating α mating factor in the absence of either small molecule. Error bars represent the standard deviation of at least three replicates. *P* values were determined by a two-tailed *t* test of the compared data sets.

Measuring Mating Pathway Activity via Halo Assays

Mating associated cell-cycle arrest was evaluated with halo assays as previously described (*46*). Briefly, halo assays were performed on cultures harboring the indicated constructs grown overnight in the appropriate dropout medium, backwards diluted into fresh medium to an OD_{600} of <0.1, and grown to an OD_{600} between 0.2 and 0.4. Each replicate was plated at a volume of 300 µl on the appropriate dropout plates. For galactose-titration halo assays, cells were plated on noninducing, nonrepressing solid medium with varying concentrations of galactose (0, 0.25, 0.5, 1, 2, and 3%). For characterization of the molecular network diverters, we plated cells on solid dropout medium containing the indicated concentration of signal molecule (theophylline or tetracycline). After plating the cells, a gradient of α mating factor was established by saturating a filter disk (2-mm diameter) of Whatman paper with

9 µl of 0.1 mg/ml α mating factor and placing the disk on the center of the plate. Cells were grown for 18 hours at 30°C and imaged via epi-white illumination with a GelDoc XR+ System (Bio-Rad). Representative images are presented from experiments performed at least in triplicate.

Images from halo assays were analyzed using ImageJ (NIH, Bethesda, MD) software analysis to extract pixel intensity at each position along a horizontal slice of the halo image by using the rectangular tool. Standard slices were centered on the filter disc. Heat maps were generated using the "HeatMap" function from MATLAB (Mathworks, Natick, MA) for the halo assays at a standard window size. To ensure that the heat map captured the changes in growth and was standardized across all maps, we excluded high-intensity data (e.g., the filter disc) and fixed the range of intensities (pixels of 120 to 200).

Calculating Relative Regulator Expression

Details are available in supplementary materials.

Evaluating Selection of Mating-Resistant Population

Details are available in supplementary materials.

Determining Resolution and Variation in Positive-Diverter Networks

Details are available in supplementary materials.

Measuring Mating Efficiencies

Details are available in supplementary materials.

Modeling of Molecular Networks Diverter Interactions with the Mating Pathway

We built a simple phenomenological model to describe the dynamic behavior of key components of our pathway: Ste4, Fus3, Msg5, and Fus1 (output). The model consists of four deterministic ordinary differential equations (ODEs 1 to 4 below), and it builds on models previously proposed in the literature (*47*–*49*). A complete description of this signaling cascade would include additional phosphorylation intermediates and scaffold proteins (*19*). However, detailed mechanistic ODE models of the MAPK pathway in *Xenopus* show that the resulting input and output behavior of this multilayered signaling cascade is equivalent to a highly cooperative activation enzymatic process (*47*). Thus, we reduced the model to a four-component system, where the unmodeled phosphorylation and dephosphorylation kinetics between Ste4, Msg5, and Fus3 are qualitatively captured by Hill functions with high Hill coefficients.

Each synthetic regulatory element in our pathway is individually modeled. We used zero-order production rates to capture the effects of constitutive promoters and switches on the native pathway. These production rates are modulated according to the strength of the switch employed. We used Hill functions to model the pathway-responsive promoter (*pFUS1*/*pFB*), which generates the positive-feedback (Ste4 activation) and negative-feedback (Msg5 activation) loops.

The model was fit to normalized *pFUS1-GFP* steady-state data. We used the results of several experimental assays, testing the effects of each individual synthetic regulatory module on the native pathway output. The steady-state data sets simultaneously used in the fitting algorithm include the response of the pathway (i) at different concentrations of pheromone (α-factor), (ii) in the presence of *pC-Ste4*, (iii) in the presence of *pC-Msg5*, (iv) in the presence of *pFB-Ste4*, (v) in the presence of *pFB-Msg5* with a range of transducers for each (ii-v). Fits were generated using MATLAB "fmincon" routine, minimizing the squared error between the numerically generated steady-state of Fus1 and the normalized measured data. ODEs were integrated using a forward Euler method. Upper and lower bounds were chosen for each parameter to guarantee positivity and boundedness of the solutions.

The parameters resulting from our fit are in general agreement with expected relative values of reaction rates for promoter activity and for phosphorylation and dephosphorylation pathways (table S3). The Mgs5-mediated maximal dephosphorylation rate of Fus3 is high relative to other rates; the efficacy of Msg5 as a strong phosphatase for Fus3 is well known (*50*, *51*), but few experimental kinetic measurements are available in the literature (*52*). Our parameter for Msg5 dephosphorylation is consistent with previous work (*52*). The half-maximal concentration of Msg5 ($K_{M,Msg5}$) is low, in agreement with our experimental observations.

$$\frac{d}{dt}[Ste4] = \beta_{Ste4} - \delta_{Ste4}[Ste4] + k_{C,Ste4}SCtc + k_{FB,Ste4}SFtc\frac{[Fus1]^{n_{pf}}}{K_{M,Fus1,pf}^{n_{pf}} + [Fus1]^{n_{pf}}} \quad (1)$$

$$\frac{d}{dt}[Fus3] = \beta_{Fus3} + k_{Ste4}\frac{[Ste4]^m}{K_{M,Ste4}^m + [Ste4]^m} + k_{\alpha}\frac{[\alpha]^n}{K_{M,\alpha}^n + [\alpha]^n} - \delta_{Fus3}[Fus3] - k_{Msg5}[Fus3]\frac{[Msg5]^q}{K_{M,Msg5}^q + Msg5^q} \quad (2)$$

$$\frac{d}{dt}[Msg5] = \beta_{Msg5} - \delta_{Msg5}[Msg5] + k_{C,Msg5}SCth + k_{FB,Msg5}SFth\frac{[Fus1]^{n_{nf}}}{K_{M,MFus1,nf}^{n_{nf}} + [Fus1]^{n_{nf}}} \quad (3)$$

$$\frac{d}{dt}[Fus1] = \beta_{Fus1} - \delta_{Fus1}[Fus1] + k_{Fus3}\frac{[Fus3]^p}{K_{M,Fus3}^p + [Fus3]^p} \quad (4)$$

References and Notes

1. R. Seger, E. G. Krebs, The MAPK signaling cascade. *FASEB J.* **9**, 726–735 (1995). pmid: 7601337
2. K. L. Pierce, R. T. Premont, R. J. Lefkowitz, Seven-transmembrane receptors. *Nat. Rev. Mol. Cell Biol.* **3**, 639–650 (2002). doi: 10.1038/nrm908; pmid: 12209124
3. A. Negro, B. K. Brar, K. F. Lee, Essential roles of Her2/erbB2 in cardiac development and function. *Recent Prog. Horm. Res.* **59**, 1–12 (2004). doi: 10.1210/rp.59.1.1; pmid: 14749494
4. Y. Y. Chen, M. C. Jensen, C. D. Smolke, Genetic control of mammalian T-cell proliferation with synthetic RNA regulatory systems. *Proc. Natl. Acad. Sci. U.S.A.* **107**, 8531–8536 (2010). doi: 10.1073/pnas.1001721107; pmid: 20421500
5. S. J. Culler, K. G. Hoff, C. D. Smolke, Reprogramming cellular behavior with RNA controllers responsive to endogenous proteins. *Science* **330**, 1251–1255 (2010). doi: 10.1126/science.1192128; pmid: 21109673
6. J. C. Anderson, E. J. Clarke, A. P. Arkin, C. A. Voigt, Environmentally controlled invasion of cancer cells by engineered bacteria. *J. Mol. Biol.* **355**, 619–627 (2006). doi: 10.1016/j.jmb.2005.10.076; pmid: 16330045
7. C. Kemmer *et al.*, Self-sufficient control of urate homeostasis in mice by a synthetic circuit. *Nat. Biotechnol.* **28**, 355–360 (2010). doi: 10.1038/nbt.1617; pmid: 20351688
8. W. Weber, M. Daoud-El Baba, M. Fussenegger, Synthetic ecosystems based on airborne inter- and intrakingdom communication. *Proc. Natl. Acad. Sci. U.S.A.* **104**, 10435–10440 (2007). doi: 10.1073/pnas.0701382104; pmid: 17551014
9. H. Ye, M. Daoud-El Baba, R. W. Peng, M. Fussenegger, A synthetic optogenetic transcription device enhances blood-glucose homeostasis in mice. *Science* **332**, 1565–1568 (2011). doi: 10.1126/science.1203535; pmid: 21700876
10. Z. Xie, L. Wroblewska, L. Prochazka, R. Weiss, Y. Benenson, Multi-input RNAi-based logic circuit for identification of specific cancer cells. *Science* **333**, 1307–1311 (2011). doi: 10.1126/science.1205527; pmid: 21885784
11. J. M. Callura, D. J. Dwyer, F. J. Isaacs, C. R. Cantor J. J. Collins, Tracking, tuning, and terminating microbial physiology using synthetic riboregulators. *Proc. Natl. Acad. Sci. U.S.A.* **107**, 15898–15903 (2010). doi: 10.1073/pnas.1009747107; pmid: 20713708
12. T. L. Deans, C. R. Cantor, J. J. Collins, A tunable genetic switch based on RNAi and repressor proteins for regulating gene expression in mammalian cells. *Cell* **130**, 363–372 (2007). doi: 10.1016/j.cell.2007.05.045; pmid: 17662949
13. H. Kobayashi *et al.*, Programmable cells: Interfacing natural and engineered gene networks. *Proc. Natl. Acad. Sci. U.S.A.* **101**, 8414–8419 (2004). doi: 10.1073/pnas.0402940101; pmid: 15159530
14. Y. Y. Chen, K. E. Galloway, C. D. Smolke, Synthetic biology: Advancing biological frontiers by building synthetic systems. *Genome Biol.* **13**, 240 (2012). doi: 10.1186/gb-2012-13-2-240; pmid: 22348749
15. D. Hanahan, R. A. Weinberg, The hallmarks of cancer. *Cell* **100**, 57–70 (2000). doi: 10.1016/S0092-8674(00)81683-9; pmid: 10647931
16. F. McCormick, Signalling networks that cause cancer. *Trends Cell Biol.* **9**, M53–M56 (1999). doi: 10.1016/S0962-8924(99)01668-2; pmid: 10611683
17. H. G. Dohlman, J. W. Thorner, Regulation of G protein-initiated signal transduction in yeast: Paradigms and principles. *Annu. Rev. Biochem.* **70**, 703–754 (2001). doi: 10.1146/annurev.biochem.70.1.703; pmid: 11395421
18. E. A. Elion, Pheromone response, mating and cell biology. *Curr. Opin. Microbiol.* **3**, 573–581 (2000). doi: 10.1016/S1369-5274(00)00143-0; pmid: 11121776
19. C. J. Bashor, N. C. Helman, S. Yan, W. A. Lim, Using engineered scaffold interactions to reshape MAP kinase pathway signaling dynamics. *Science* **319**, 1539–1543 (2008). doi: 10.1126/science.1151153; pmid: 18339942

20. N. T. Ingolia, A. W. Murray, Positive-feedback loops as a flexible biological module. *Curr. Biol.* **17**, 668–677 (2007). doi: 10.1016/j.cub.2007.03.016; pmid: 17398098
21. S. H. Park, A. Zarrinpar, W. A. Lim, Rewiring MAP kinase pathways using alternative scaffold assembly mechanisms. *Science* **299**, 1061–1064 (2003). doi: 10.1126/science.1076979; pmid: 12511654
22. S. D. Santos, P. J. Verveer, P. I. Bastiaens, Growth factor-induced MAPK network topology shapes Erk response determining PC-12 cell fate. *Nat. Cell Biol.* **9**, 324–330 (2007). doi: 10.1038/ncb1543; pmid: 17310240
23. E. Franco, F. Blanchini, Structural properties of the MAPK pathway topologies in PC12 cells. *J. Math. Biol.* (2012). doi: 10.1007/s00285-012-0606-x
24. M. N. Win, C. D. Smolke, A modular and extensible RNA-based gene-regulatory platform for engineering cellular function. *Proc. Natl. Acad. Sci. U.S.A.* **104**, 14283–14288 (2007). doi: 10.1073/pnas.0703961104; pmid: 17709748
25. R. G. Palpant, R. Steimnitz, T. H. Bornemann, K. Hawkins, The Carter Center Mental Health Program: Addressing the public health crisis in the field of mental health through policy change and stigma reduction. *Prev. Chronic Dis.* **3**, A62 (2006). pmid: 16539803
26. M. Osterberg *et al*., Phenotypic effects of membrane protein overexpression in *Saccharomyces cerevisiae*. *Proc. Natl. Acad. Sci. U.S.A.* **103**, 11148–11153 (2006). doi: 10.1073/pnas.0604078103; pmid: 16847257
27. S. A. Chapman, A. R. Asthagiri, Quantitative effect of scaffold abundance on signal propagation. *Mol. Syst. Biol.* **5**, 313 (2009). doi: 10.1038/msb.2009.73; pmid: 19888208
28. H. B. Fraser, A. E. Hirsh, G. Giaever, J. Kumm, M. B. Eisen, Noise minimization in eukaryotic gene expression. *PLoS Biol.* **2**, e137 (2004). doi: 10.1371/journal.pbio.0020137; pmid: 15124029
29. J. Stelling, E. D. Gilles, F. J. Doyle 3rd, Robustness properties of circadian clock architectures. *Proc. Natl. Acad. Sci. U.S.A.* **101**, 13210–13215 (2004). doi: 10.1073/pnas.0401463101; pmid: 15340155
30. J. Stelling, U. Sauer, Z. Szallasi, F. J. Doyle 3rd, J. Doyle, Robustness of cellular functions. *Cell* **118**, 675–685 (2004). doi: 10.1016/j.cell.2004.09.008; pmid: 15369668
31. A. Eldar *et al*., Robustness of the BMP morphogen gradient in *Drosophila* embryonic patterning. *Nature* **419**, 304–308 (2002). doi: 10.1038/nature01061; pmid: 12239569
32. G. Stoll, M. Bischofberger, J. Rougemont, F. Naef, Stabilizing patterning in the *Drosophila* segment polarity network by selecting models in silico. *Biosystems* **102**, 3–10 (2010). doi: 10.1016/j.biosystems.2010.07.014; pmid: 20655356
33. E. C. O'Shaughnessy, S. Palani, J. J. Collins, C. A. Sarkar, Tunable signal processing in synthetic MAP kinase cascades. *Cell* **144**, 119–131 (2011). doi: 10.1016/j.cell.2010.12.014; pmid: 21215374
34. T. M. Thomson *et al*., Scaffold number in yeast signaling system sets tradeoff between system output and dynamic range. *Proc. Natl. Acad. Sci. U.S.A.* **108**, 20265–20270 (2011). doi: 10.1073/pnas.1004042108; pmid: 22114196
35. J. C. Liang, A. L. Chang, A. B. Kennedy, C. D. Smolke, A high-throughput, quantitative cell-based screen for efficient tailoring of RNA device activity. *Nucleic Acids Res.* **40**, e154 (2012). doi: 10.1093/nar/gks636; pmid: 22810204
36. A. Becskei, L. Serrano, Engineering stability in gene networks by autoregulation. *Nature* **405**, 590–593 (2000). doi: 10.1038/35014651; pmid: 10850721
37. C. L. Beisel, C. D. Smolke, Design principles for riboswitch function. *PLOS Comput. Biol.* **5**, e1000363 (2009). doi: 10.1371/journal.pcbi.1000363; pmid: 19381267
38. C. J. Marshall, Specificity of receptor tyrosine kinase signaling: Transient versus sustained extracellular signal-regulated kinase activation. *Cell* **80**, 179–185 (1995). doi: 10.1016/0092-8674(95)90401-8; pmid: 7834738
39. C. Banerjee *et al*., Differential regulation of the two principal Runx2/Cbfa1 N-terminal isoforms in response to bone morphogenetic protein-2 during development of the osteoblast phenotype. *Endocrinology* **142**, 4026–4039 (2001). doi: 10.1210/en.142.9.4026; pmid: 11517182
40. Y. Yuan *et al*., Alternative splicing and gene duplication differentially shaped the regulation of isochorismate synthase in *Populus* and *Arabidopsis*. *Proc. Natl. Acad. Sci. U.S.A.* **106**, 22020–22025 (2009). doi: 10.1073/pnas.0906869106; pmid: 19996170
41. U. S. Bhalla, P. T. Ram, R. Iyengar, MAP kinase phosphatase as a locus of flexibility in a mitogen-activated protein kinase signaling network. *Science* **297**, 1018–1023 (2002). doi: 10.1126/science.1068873; pmid: 12169734
42. W. Wu, T. Pew, M. Zou, D. Pang, S. D. Conzen, Glucocorticoid receptor-induced MAPK phosphatase-1 (MPK-1) expression inhibits paclitaxel-associated MAPK activation and contributes to breast cancer cell survival. *J. Biol. Chem.* **280**, 4117–4124 (2005). doi: 10.1074/jbc.M411200200; pmid: 15590693
43. W. Wu *et al*., Microarray analysis reveals glucocorticoid-regulated survival genes that are associated with inhibition of apoptosis in breast epithelial cells. *Cancer Res.* **64**, 1757–1764 (2004). doi: 10.1158/0008-5472.CAN-03-2546; pmid: 14996737
44. S. Srikanth, C. C. Franklin, R. C. Duke, R. S. Kraft, Human DU145 prostate cancer cells overexpressing mitogen-activated protein kinase phosphatase-1 are resistant to Fas ligand-induced mitochondrial perturbations and cellular apoptosis. *Mol. Cell. Biochem.* **199**, 169–178 (1999). doi: 10.1023/A:1006980326855; pmid: 10544965
45. J. Y. Wang, C. H. Lin, C. H. Yang, T. H. Tan, Y. R. Chen, Biochemical and biological characterization of a neuroendocrine-associated phosphatase. *J. Neurochem.* **98**, 89–101 (2006). doi: 10.1111/j.1471-4159.2006.03852.x; pmid: 16805799
46. G. F. Sprague Jr., Assay of yeast mating reaction. *Methods Enzymol.* **194**, 77–93 (1991). doi: 10.1016/0076-6879(91)94008-Z; pmid: 2005823
47. C. Y. Huang, J. E. Ferrell Jr., Ultrasensitivity in the mitogen-activated protein kinase cascade. *Proc. Natl. Acad. Sci. U.S.A.* **93**, 10078–10083 (1996). doi: 10.1073/pnas.93.19.10078; pmid: 8816754
48. D. Angeli, J. E. Ferrell Jr., E. D. Sontag, Detection of multistability, bifurcations, and hysteresis in a large class of biological positive-feedback systems. *Proc. Natl. Acad. Sci. U.S.A.* **101**, 1822–1827 (2004). doi: 10.1073/pnas.0308265100; pmid: 14766974
49. W. Kolch, M. Calder, D. Gilbert, When kinases meet mathematics: The systems biology of MAPK signalling. *FEBS Lett.* **579**, 1891–1895 (2005). doi: 10.1016/j.febslet.2005.02.002; pmid: 15763569
50. X. L. Zhan, R. J. Deschenes, K. L. Guan, Differential regulation of FUS3 MAP kinase by tyrosine-specific phosphatases PTP2/PTP3 and dual-specificity phosphatase MSG5 in *Saccharomyces cerevisiae*. *Genes Dev.* **11**, 1690–1702 (1997). doi: 10.1101/gad.11.13.1690; pmid: 9224718
51. J. Andersson, D. M. Simpson, M. Qi, Y. Wang, E. A. Elion, Differential input by Ste5 scaffold and Msg5 phosphatase route a MAPK cascade to multiple outcomes. *EMBO J.* **23**, 2564–2576 (2004). doi: 10.1038/sj.emboj.7600250; pmid: 15192700
52. B. Kofahl, E. Klipp, Modelling the dynamics of the yeast pheromone pathway. *Yeast* **21**, 831–850 (2004). doi: 10.1002/yea.1122; pmid: 15300679

Acknowledgments: We thank D. Endy, J. Michener, A. Chang, and Y.-H. Wang for comments on the manuscript; J. Liang for technical guidance with RNA transducers; and R. Yu and S. Chapman for discussions on mating assays. This work was supported by funds from the NIH (grant to C.D.S.), NSF (grant to C.D.S.), Defense Advanced Research Projects Agency (grant to C.D.S.), and the Bill and Melinda Gates Foundation (grant to C.D.S.). K.E.G. and C.D.S. designed the study and experiments; K.E.G. performed experiments; E.F. and K.E.G. designed and constructed the model; and C.D.S. and K.E.G. analyzed and discussed all results and wrote the manuscript.

Supplementary Materials

www.sciencemag.org/content/341/6152/1235005/suppl/DC1
Materials and Methods
Supplementary Text
Figs. S1 to S14
Tables S1 to S17
References (*53*–*60*)

9 January 2013; accepted 24 July 2013
Published online 15 August 2013;
10.1126/science.1235005